J. Biophoton. **3**, No. 7, 446–454 (2010) / **DOI** 10.1002/jbio.200900089

Journal of BIOPHOTONICS

FULL ARTICLE

PALM imaging and cluster analysis of protein heterogeneity at the cell surface

Dylan M. Owen, Carles Rentero, Jérémie Rossy, Astrid Magenau, David Williamson, Macarena Rodriguez, and Katharina Gaus*

Centre for Vascular Research, University of New South Wales, High Street, Sydney, New South Wales 2052, Australia

Received 9 December 2009, revised 19 January 2010, accepted 20 January 2010
Published online 11 February 2010

Key words: PALM, STORM, lipid rafts, membrane microdomains, immune synapse, Lck

The authors employed photoactivatable localization microscopy (PALM) and direct stochastic optical reconstruction microscopy (dSTORM) imaging and image analysis based on Ripley's *K*-function to quantify the distribution and heterogeneity of proteins at the cell plasma membrane. The membrane targeting sequence of the N-terminal region of the T cell receptor-pathway kinase Lck fused to the photo-convertible fluorescent protein tdEos (Lck_{N10}-tdEos), clusters into sub-100 nm regions which cover ~7% of the cell surface. 2-channel PALM imaging of Lck_{N10}-tdEos and the N-terminus of the kinase Src (Src_{N15}-PS-CFP2) are demonstrated. Finally, T cell microclusters at the immune synapse are imaged at super-resolution using dSTORM, showing that conventional TIRF images contain unresolved, small clusters. These methods are generally applicable to other cell and fluorophore systems to quantify 2-D molecular clustering at nanometer scales.

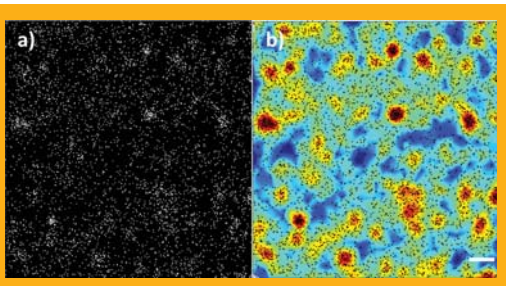

PALM image (**a**) and quantitative cluster map (**b**) based on Ripley's *K*-function of the membrane targeting sequence of the kinase Lck (Lck_{N10}-tdEos) in the plasma membrane of fixed HeLa cells. Scale bar 200 nm.

1. Introduction

Photoactivatable localization microscopy (PALM) and stochastic optical reconstruction microscopy (STORM) were first demonstrated in 2006 as methods for producing super-resolution fluorescence images [1, 2]. Both PALM and STORM can generate images with a spatial resolution of tens of nanometers – significantly higher than conventional microscopy [3]. The PALM method is based on the use of photo-convertible or photo-activatable fluorescent proteins of which a wide range are now available [4]. In this study, we use the tandem-dimer photo-convertible protein tdEos, a variant of wtEosFP from the coral *Lobophyllia hemprichii* [5] or PS-CFP2 for dual color imaging. In the unconverted state tdEos is excited at 506 nm and emission is at 516 nm (green). Upon irradiation with 405 nm light, the protein converts to red fluorescence (excitation 569 nm, emission 581 nm) due to cleavage at His61 leading to the

* Corresponding author: e-mail: dylan.owen@unsw.edu.au

incorporation of a second imidazole ring into the conjugated HYG chromophore.

By illuminating the sample with low intensity 405 nm radiation and imaging the red-fluorescent species with single-molecule sensitivity, the density of observed molecules can be made to be less than one molecule per diffraction-limited observation volume. This permits the position of the molecule, which is the centre of the point-spread-function (PSF), to be located. To facilitate single-molecule imaging, total internal reflection fluorescence (TIRF) microscopy is used [6]. Evanescent wave excitation provides ~100 nm optical sectioning, thus reducing out of focus background and increasing signal-to-noise levels. Figure 1 shows an illustration of the PALM method applied to Lck_{N10} or Src_{N15} fluorescent fusion constructs at the cell plasma membrane.

STORM, employed here as direct STORM (dSTORM) [7], relies on the reversible photo-switching of conventional fluorophores, in this case Cy5, into a dark state when excited using 633 nm laser radiation. This is achieved by means of a 'switching buffer' that allows a broad palate of conventional dyes to cycle between 'on' and 'off' states [7, 8]. This technique is in contrast to conventional STORM in which two small molecule dyes in close proximity are required to achieve photo-switching which can lead to an undesirable increase in the complexity of the sample preparation. Switching of Cy5 back out of the dark or 'off' state in dSTORM is achieved by exposure to low intensities of 488 nm laser light. This method allows the use of immunostaining to visualize proteins of interest.

PALM and STORM are unique in that an image is built up molecule by molecule. Hence PALM and STORM images contain information about the 2-dimensional molecular distribution of proteins within the plasma membrane. Ripley's *K*-function is a statistical method for analyzing the clustering of points in a 2-dimensional distribution [9]. Recently, it has been shown theoretically to be appropriate for extracting properties of domains in the plasma membrane [10]. The method has also been used extensively in the quantification of clustering in electron microscopy images of labeled proteins at the plasma membrane, for example Ras [11].

Lck is a 56 kD protein tyrosine kinase of the Src-family which is involved in numerous signalling cascades including in the early T-cell receptor signaling pathway. The protein is targeted to the plasma membrane by three post-translational lipid modifications at the N-terminus. These are a myristoylation site at glycine 2 and two palmitoylation sites at cysteins 3 and 5. It is thought that these lipid modifications further serve to target Lck to ordered membrane lipid microdomains or lipid rafts. Lipid rafts have been shown to be important in the formation of the immunological synapse between T

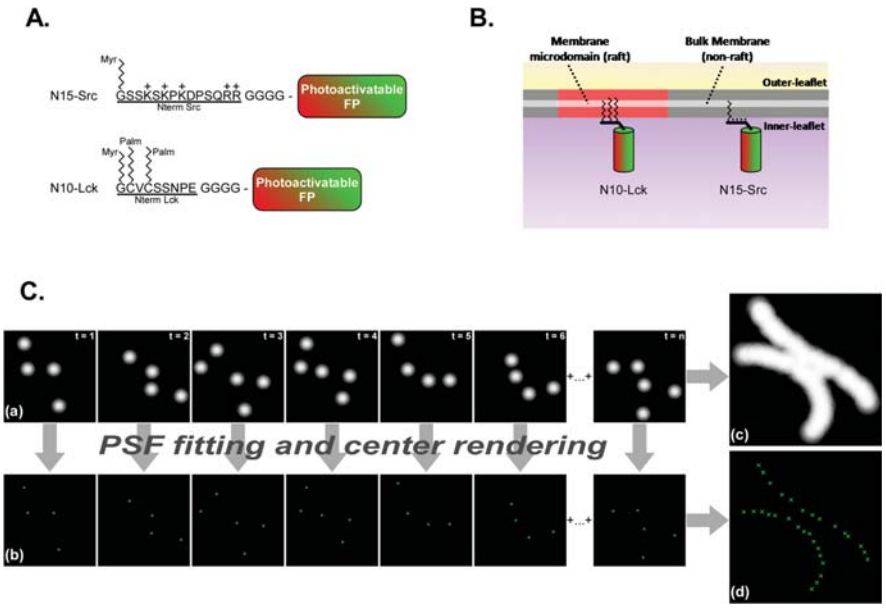

Figure 1 (online color at: www.biophotonics-journal.org) PALM imaging. (**A**) The photo-convertible protein tdEos is targeted to the membrane by fusion to the peptide Lck_{N10} which has 3 post-translational acyl modifications or Src_{N15} which is only myristoylated. (**B**) Both peptide sequences target the protein to the plasma membrane but they may reside in different membrane domains. (**C**) Prior to conversion, the protein exhibits green fluorescence but exposure to 405 nm radiation produces a red chromophore. From images of this red chromophore, the centroid of the PSF can be found, allowing the molecule to be localized with high precision. Repeating this process many times assembles a single super resolution image.

cells and their targets and therefore may be important in regulating the distribution of Lck at the cell surface [12].

Much of the controversy surrounding the lipid raft hypothesis [13] stems from our inability to observe these domains directly due to spatial and temporal resolution restrictions of available microscopes. Here, we used PALM microscope and Ripley's *K*-function analysis to examine the distribution of the first 10 amino acids of N-terminal tail of Lck (Lck_{N10}) fused to tdEos in HeLa cells. We generated cluster maps from which important cluster parameters about the clustering behavior were extracted. We also demonstrated 2-color PALM and cluster analysis of Lck_{N10} together with the first 15 amino acids of the N-terminus the kinase Src. (Src_{N15}). Like Lck, Src kinases are involved in many signaling processes including G-protein coupled receptor signaling pathways. The N-terminus peptide is only myristoylated with apparently no preference for lipid rafts.

The T cell immune synapse is a stable cell-cell junction formed between a T cell and an antigen presenting cell (APC) [14–16]. T cell receptor (TCR) triggering results in the formation of TCR microclusters at the immunological synapse, which include clusters of the scaffolding protein Linker for Activation of T cells (LAT) [16]. These TCR LAT clusters facilitate the early T cell signalling events and are essential for T cell activation [18–21]. Despite their functional importance, due to spatial resolution limitations of conventional fluorescence microscopes, key parameters such as the fraction of LAT molecules found in microclusters remain unknown.

We applied the dSTORM method to the analysis of microclusters of phosphorylated LAT at the T cell immunological synapse for the first time. This is achieved by activating Jurkat T cells on glass coverslips using antibodies to the T cell receptor molecule CD3 followed by fixation and immune-staining with antibodies specific for pLAT191. In this system, we were able to extract key quantitative parameters describing the organization of these entities.

2. Materials and methods

2.1 Sample preparation

HeLa cells were cultured on piranha (70% H_2SO_4, 30% H_2O_2)-cleaned glass coverslips in DMEM media (Gibco, Invitrogen, Carlsbad, CA) supplemented with 10% foetal calf serum (FCS) at 37 °C in a 5% CO_2 atmosphere.

The 10-amino acid N-terminus region of Lck was fused to the photo-switchable fluorescent protein tdEos or PS-CFP2 via a short 4 amino-acid (GGGG) linker (Lck_{N10}-tdEos or Src_{N15}-PS-CFP2). This region contains the membrane targeting sequence (1 myristoylation and 2 palmitoylation sites) which targets the construct to detergent-resistant membranes similarly to the full-length protein [23, 24]. The constructs were transfected into HeLa cells 24 hours prior to imaging using lipofectamine LTX (Invitrogen, Carlsbad, CA).

The cells were washed twice with phosphate-buffered saline (PBS) and fixed using 4% paraformaldehyde (PFA) at 37 °C for 20 minutes before being washed again with PBS. For imaging, cells were mounted in POC-R2 chambers (PeCon GmbH, Erbach, Germany).

For dSTORM, Jurkat E6.1 T cells were cultured in RPMI1640 media (Gibco, Invitrogen, Carlsbad, CA) supplemented with 10% FCS at 37 °C in a 5% CO_2 atmosphere. Cells were allowed to form synapses on Piranha-cleaned glass coverslips which were coated by 20 μg/mL anti-CD3 antibody (OKT3, Ebioscience, San Diego, CA) for 10 min at 37 °C. Cells were then fixed with 4% PFA for another 10 min at 37 °C, permeabilized and stained with a rabbit anti-pLat191 antibody (Invitrogen, Carlsbad, CA) and a goat Cy5 conjugated anti-rabbit secondary antibody (Jackson Immunoresearch, West Grove, PA).

Antibody stained cells were imaged in an oxygen scavenging buffer (0.1 mg/ml glucose oxidase, 0.1 mg/ml horseradish peroxidase, 1% β-mercaptoethanol, 25 mM Hepes, 25 mM glucose, 5% glycerol in PBS, pH 8) in a sealed in a POC-R2 chamber (PeCon GmbH, Erbach, Germany). Cells were imaged with surface-immobilized 100 nm colloidal gold beads that allow correction for sample drift during the acquisition.

2.2 Microscopy

PALM images were acquired on a prototype PALM temperature-controlled inverted fluorescence microscope (Carl Zeiss GmbH, Jena, Germany) with TIRF illumination and a 1.45NA 63X oil-immersion TIRFM objective. Photo-conversion was achieved using a diode-pumped solid state laser (DPSSL) operating at 405 nm. tdEos was excited using a DPSSL operating at 488 nm before conversion and 561 nm after conversion. PS-CFP2 was also converted at 405 nm and imaged after photoconversion with 488 nm. Laser powers used for imaging were approximately 10 mW (in the incidence beam) at 561 nm and approximately 160 nW at 405 nm at the sample. The penetration depth of the evanescent field (1/e) was calculated theoretically to be

~100 nm for the activation laser and ~140 nm for the imaging laser. For dSTORM of Cy5, the lasers lines used were 633 nm (15 mW) (for imaging) and 488 nm (0.1–1 mW) (for recovery of the 'on' state), both from DPSSLs. Images were captured using an Andor iXon DU-897D EMCCD camera (Andor Technology Plc, Belfast, UK) operating at −50 °C with an integration time of 0.02 s and with an additional 1.6X magnification before the camera such that the final image pixel size was 100 nm. PALM images were reconstructed from a series of 15,000 TIRF images using Zeiss Zen software (Carl Zeiss GmbH, Jena, Germany).

2.3 Cluster analysis

The data generated by the PALM microscope is of the form of a table of $x-y$ co-ordinates of all the detected events. This can be used to construct a 2-D spatial point pattern of the molecular distribution. In this case, the molecular density was approximately 1500 molecules per square micron. For analysis, $2 \times 2\ \mu m^2$ areas were selected. Ripley's K-function was then calculated using SpPack [22] as:

$$\hat{K}(r) = A \sum ((i=1) \to n) \sum ((i=1) \to n)\ (\delta_{ij}/n^2)$$

where $\delta_{ij} = 1$ if $\delta_{ij} < r$, otherwise 0

Where A is the area, n is the number of points, r is the spatial scale (radius) for the K-function calculation and δ_{ij} is the distance between points i and j. This essentially counts the number of other points encircled by concentric rings centered on each point. This function is then linearized to generate the L-function according to:

$$L(r) = \sqrt{((K(r))/\pi)}$$

For a random distribution of points, $L(r) = r$ and therefore we plot $L(r) - r$ (sometimes termed the H-function) against r such that a random distribution has $L(r) - r =$ zero for all r. Therefore, for scales at which the distribution is more clustered than would be expected of a random distribution, $L(r) - r$ is positive, whereas $L(r) - r$ is negative if the points are less clustered than would be expected for random events. Edge-effects were negated by weighting edge points and cropping image edges after the calculation.

Values of $L(r)$ generated for each point were used to produce a map of clustering by interpolating a surface plot with $L(r)$ as the z-axis (color scale). Spatial interpolation was performed with a resolution of 10 nm using MatLAB (The Mathworks Inc., Natick, MA) to generate a 2-dimensional cluster map. This cluster map was then thresholded to produce a binary cluster map from which the number of clusters, cluster size and shape etc. could be extracted.

3. Results and discussion

Fibroblasts were transfected with Lck_{N10}-tdEos and the samples excited under TIRF illumination with ~160 nW 405 nm for photo-conversion of tdEos nm and ~10 mW 561 nm to image the converted red fluorescent tdEos. Figure 2a) shows the TIRF image and Figure 2b) shows a representative PALM image of Lck_{N10}-tdEos. The zoomed regions in each case demonstrate the increased resolution available from PALM microscopy. In Figure 2c), the histogram of molecular localization precision is shown, demonstrating that the peak localization precision is ~20 nm. The histogram was calculated according to a method previously described, taking into account the photon count for each molecule, noise, the full width half maximum of the observed point-spread-function and the camera pixel size [25].

The averaged Ripley's $L(r) - r$ plot for the whole image is displayed in Figure 2d). From this plot it is clearly evident that the point-pattern displays a highly clustered nature. The value of $L(r) - r$ rises significantly above zero indicating clustering (more points are being encircled by concentric circles, centered on each point, than would be expected for a random distribution for circle radii between 0 and 500 nm). The spatial scale, at which Lck_{N10}-tdEos clusters to the highest degree, is 70 nm, however, the protein remains significantly clustered up to scales of several hundred nanometers. Beyond approximately 500 nm, the points become less clustered than would be expected of a random distribution (less points are being encircled at these radii), resulting in the values of $L(r) - r$ in the plot becoming negative.

An expanded $2 \times 2\ \mu m^2$ area from Figure 2b) is displayed in Figure 2e). From this spatial point-pattern, Figure 2f) shows a 2-D map of clustering based on Ripley's K-function analysis of each point. For every point, concentric circles were drawn and the number of encircled points counted and comparing this value to a random distribution. This image was calculated by assigning each point a value for the number of other points encircled within a 50 nm radius circle. Once each point had been assigned this value, a color coded surface was interpolated to generate the cluster map. Red represents highly clustered regions whereas green and blue colors denote low values for clustering. From this map it can be seen that the construct is highly clustered on spatial scales below the resolution of a standard fluorescence microscope.

Finally, Figure 2g) shown the binary cluster map generated by applying a threshold to Figure 2f). The

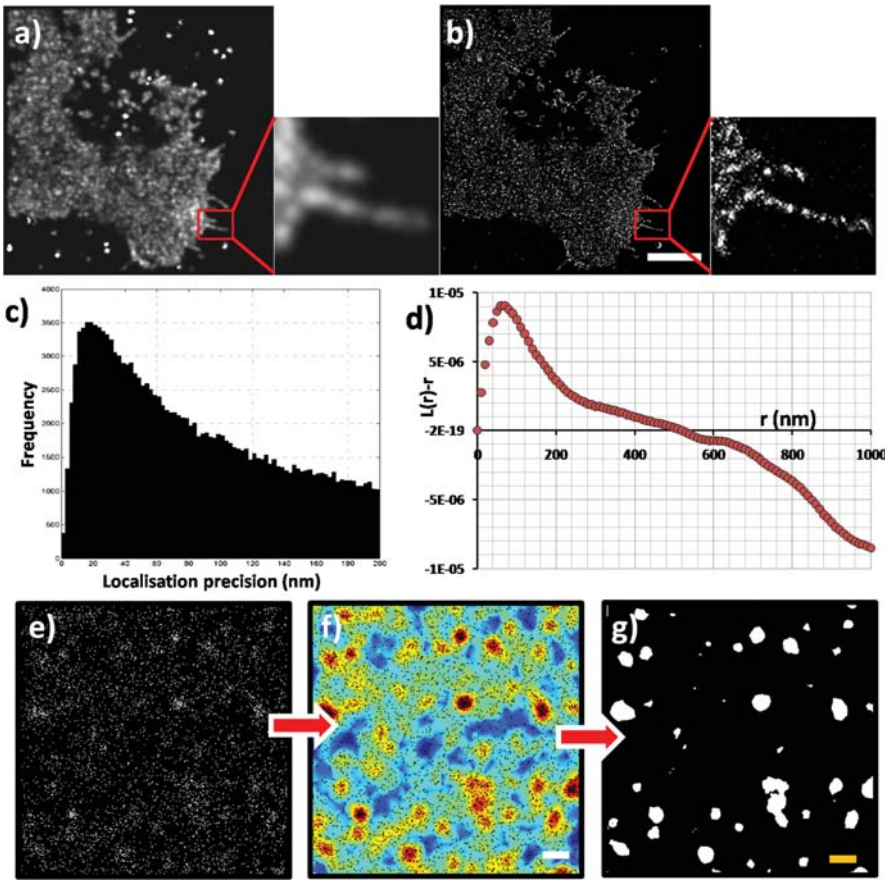

Figure 2 (online color at: www.biophotonics-journal.org) PALM microscopy and cluster analysis of Lck_{N10}-tdEos. (**a**) TIRF image and zoomed region. (**b**) PALM image and zoomed region (scale bar 5 μm) showing increased image resolution of PALM imaging. (**c**) Localization precision histogram of the PALM image identifies peak localization at ~20 nm. Localization precisions were calculated as described elsewhere [23]. (**c**) Ripley's *K*-function plot showing peak clustering scales at ~70 nm and clustering above the level expected for a random distribution on length scales up to 500 nm. (**e**) Expanded $2 \times 2\ \mu m^2$ region of the PALM image showing point distribution of molecules. (**f**) Interpolated cluster map based on Ripley's *K*-function analysis indicating a highly clustered distribution (red areas) (scale bar 200 nm). (**g**) Binary cluster image generated from Fig. 2f) using a threshold. From this image the number of clusters, cluster size, shape and other parameters can be extracted.

threshold was set at 60% of the peak value. From this binary map, a number of important experimental parameters can be extracted. For example, this $2 \times 2\ \mu m^2$ area contains 54 cluster domains, which cover 6.8% of the total area. On average each molecular cluster has an area of 50,370 nm^2, which, if they were circular, would indicate an average radius of 126 nm. In fact, the clusters have a circularity of 0.71 (measured as the ratio of perimeter to area such that a perfect circle equals 1) indicating they are relatively circular. 58% of molecules are found in these clusters meaning that the molecular density inside these regions (12,202 molecules/μm^2) is over 8 times higher than that outside (1,407 molecules/μm^2).

We next ran simulated data to confirm that the image analysis method does return the correct parameters. Point data was simulated with set cluster positions, cluster sizes and densities on a randomly distributed background of a set density. Figure 3 shows 2 examples of the simulated data, each containing a single (uniform) circular cluster. The cluster size was set to 70 nm and 200 nm, with the density ratio in/out of clusters as 8 : 1 (roughly similar to that observed for the Lck_{N10}-tdEos clusters in HeLa cells).

The 70 nm simulated clusters resulted in a cluster size of 71.4 nm after the analysis process, an overestimation by 2%. The 200 nm clusters resulted in an output of 210 nm, a 5% error. Cluster circularity was 0.845 and 0.804 respectively (calculated, as above, as the ratio of area to perimeter). Given the relatively

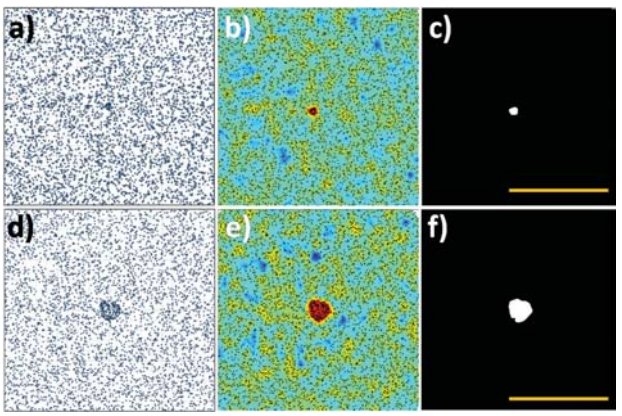

Figure 3 (online color at: www.biophotonics-journal.org) Simulated cluster data of 70 nm (**a**)–(**c**) and 200 nm (**d**)–(**f**) scale uniform circular clusters. (**a**) and (**d**) simulated point-patterns based on a uniform circle of high density points over a uniform background of low density points. (**b**) and **e**) quantitative cluster maps of these distributions showing detection of the simulated cluster. (**c**) and (**f**) binary cluster maps which allow the cluster size to be extracted (scale bar 1 μm).

small overestimation of cluster sizes, we conclude that the method is appropriate for the analysis of cluster sizes in cell membranes. Other simulated parameters (data not shown) also returned accurate values. Further, the simulated data indicated that the Lck_{N10}-tdEos cluster size in HeLa cells (Figure 2) is likely to be approximately 120 nm.

After confirming the validity of the method, we went on to demonstrate 2-channel PALM and cluster analysis. HeLa cells were transfected with both Lck_{N10}-tdEos and Src_{N15}-PS-CFP2 simultaneously. Src_{N15} is targeted to the non-raft fraction during detergent resistant membrane preparations [23, 24]. These were imaged by PALM sequentially, with tdEos imaged as described above. Note that chromatic aberration was not corrected for in this data. PS-CFP2 was also photo-converted using 405 nm irradiation but was imaged using 488 nm light. The quantitative cluster mapping was then performed on each data set individually. The rainbow color map for the cluster map (shown in Figure 2f) was replaced by either a green (Src_{N15}) or red (Lck_{N10}) monochrome color scale representing the cluster value. These two maps are then merged which allowed us to determine whether clusters of each protein are overlapped and quantify the degree of co-clustering. An example of this merged two-color cluster map is shown in Figure 4. From these data, we determine that clusters of Lck_{N10}-tdEos and Src_{N15}-PS-CFP2 were not significantly overlapped and indeed may be excluded from one another.

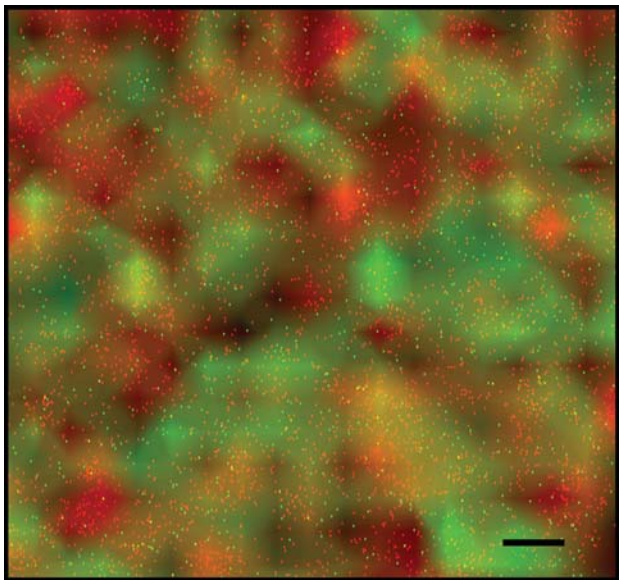

Figure 4 (online color at: www.biophotonics-journal.org) 2-color PALM clustering map showing overlaid Lck_{N10}-tdEos (red) and Src_{N15}-PS-CFP2 (green) which exist in mainly non-overlapping clusters. (Scale bar 200 nm).

For example, only just over 2% of Lck_{N10} molecules were found to reside in areas containing clustering as defined by the Src_{N15} molecular distribution, despite these clusters accounting for 9% of the total image area.

We then used dSTORM to image T cell microclusters at the immunological synapse (Figure 5). To activate T cells, clean coverglass was coated with anti-CD3 antibodies and incubated with T cells for 10 minutes. Once engaged, the antibodies cause the adhesion of the T cells to the coverglass and trigger T cell signaling. Signaling is mediated by the formation of TCR microclusters that contain the scaffolding protein, LAT [19]. Once associated with TCR microclusters, LAT is phosphorylated by the kinase ZAP-70 at the tyrosine 191. Figure 5 shows TIRF, dSTORM and a quantitative cluster map of (pY191)LAT at the T cell immunological synapse formed between a Jurkat T cell and an anti-CD3-coated glass coverslip.

In the conventional TIRF image (Figure 5a), T cell microclusters can be observed as bright punctuate structures on an otherwise dark background. In contrast, dSTORM images and cluster analysis identified TCR microclusters that were unresolved in the TIRF images or were in fact made up of several smaller entities (example marked by a red circle in Figure 5b and d). Further, the dSTORM data also shows that some clusters were formed by highly clustered molecules, where as others show a more diffuse pattern (example marked by a green circle in Figure 5b and d). These different TCR microclusters were of course indistinguishable when viewed with standard optical resolutions of TIRF microscopy. The different patterns within pLAT clusters may derive from distinct populations of microclusters. For example, it has been speculated that some may be surface microclusters whereas others are located on sub-synaptic membrane vesicles (D. M. Davis *et al.*, unpublished observations). In the conventional TIRF zoom (Figure 5b) (resolution ~250 nm), there were of the order of 20 pLAT clusters within the imaged area (3 × 5 μm). The quantitative analysis (Figure 5d) identifies around 30 clusters in the same area, indicating that the diffraction-limited TIRF imaging commonly used to study T cell microclusters may underestimate the number of clusters by up to 50%. The quantitative nature of the analysis allows us to determine that that these clusters contain approximately 81% of the pLAT molecules in the image. Because dSTORM produces multiple localizations from each fluorophore, it was not possible to determine the absolute number of molecules in the field of view. As the localization precision (10–20 nm) is much smaller than the cluster size (~100 nm) the multiple localizations have the effect of only slightly reducing the resolution of the final image.

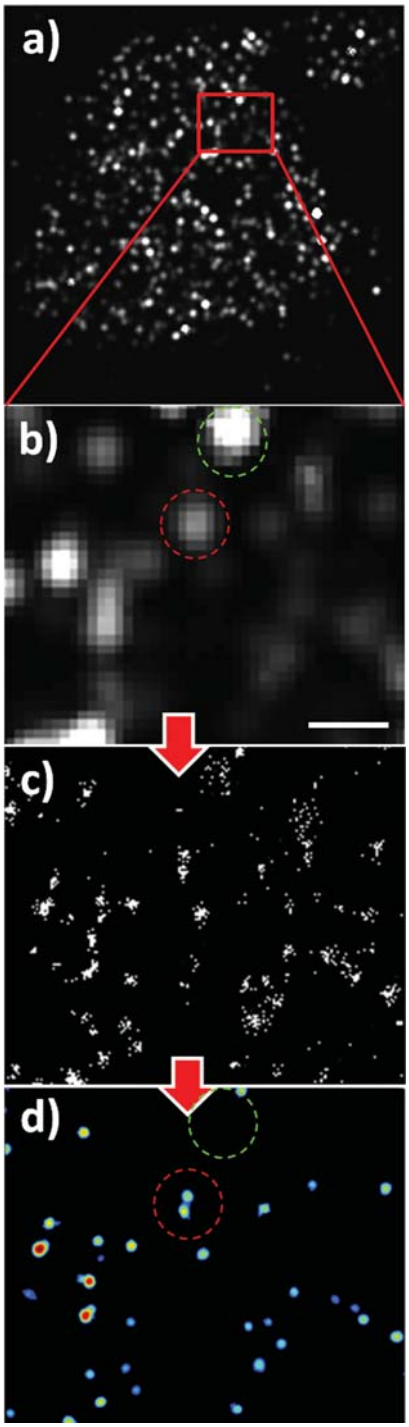

Figure 5 (online color at: www.biophotonics-journal.org) dSTORM and cluster analysis of T cell microclusters of pLAT at the immunological synapse formed on anti-CD3 coated coverslips. (**a**) Conventional TIRF image. (**b**) Zoomed region with an example of T cell microclusters (red and green circles) (**c**) Raw dSTORM image showing molecular localization and (**d**) quantitative cluster map illustrating how the microcluster circled in red is in fact two distinct entities while the one circled in green is a more diffuse molecular aggregate (scale bar 1 μm).

4. Conclusion

We have demonstrated that super-resolution PALM and dSTORM imaging and quantitative cluster mapping and analysis is a powerful quantitative tool to determine protein distributions at the cell surface. We have found that the N-terminal acylated tail of Lck, fused to the photo-convertible protein tdEos, is clustered at the plasma membrane. These clusters are of the order of 120 nm in size (clusters between 20 and 190 nm show $L(r) - r$ values above 50% of the peak and $L(r) - r$ remains positive (clustered) up to length scales of 510 nm), contain 58% of the molecules and cover approximately 7% of the cell surface. The validity of the method has been tested using simulated data.

We have further used 2 color PALM microscopy to compare the distribution of two different membrane targeting sequences: Lck_{N10} and Src_{N15}. While we find that both of these proteins are clustered into sub-resolution domains, the clusters of each protein do not significantly overlap. Given the small size of membrane domains, at least in resting cells, it is likely that PALM imaging will be a suitable approach to determine the distribution of raft and non-raft proteins at the plasma membrane of fixed cells.

Finally, we have imaged T cell microclusters of the phosphorylated scaffolding protein LAT at the immunological synapse using dSTORM. We find previously unseen diversity in the size and molecular density of these protein microclusters.

In conclusion, our proof-of-principle study shows that PALM and dSTORM imaging and quantitative cluster analysis can be used to enhance our understanding of the heterogeneity of cell surface proteins.

Acknowledgements The authors acknowledge funding from the Australian Research Council (ARC) and Human Frontier Science Program (HFSP).

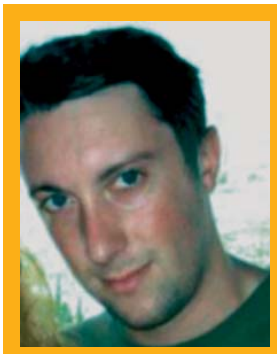

Dylan Owen received a degree in Physics, an MRes in Protein and Membrane Chemical Biology and a Ph.D. in Biomedical Optics from Imperial College London, UK. His work has concentrated on the use of novel fluorescence microscopy, especially spectrally resolved microscopy and FLIM techniques to study the organization of the cell plasma membrane. Since finishing his Ph.D. and moving to the University of New South Wales, Australia as a postdoc, he has worked on single-molecule methods (PALM and FCS) to study organization and dynamics at the cell membrane.

Carles Rentero received a degree in Biology and Biotechnology in 1999 and a Ph.D. degree in Biology in 2004 from the University of Barcelona, Spain. After a brief post-doctoral position at Faculty of Medicine of the University of Barcelona, he joined the Membrane Biology group at the University of New South Wales as post-doctoral researcher in 2006. There he worked on the study of membrane structure, cell signalling and super-resolution microscopy approaches. He is now a senior post-doctoral fellow at Faculty of Medicine, University of Barcelona working on the interactions between signalling pathways, cell membranes and the cytoskeleton.

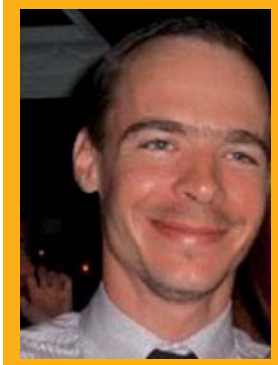

Jeremie Rossy received an MSci. in Biochemistry from the University of Geneva, Switzerland in 2002. He received his Ph.D. from the University of Bern in 2008 for a study of the membrane-cytoskeleton relationship in migrating cancer cells and lymphocytes. He has just started his first post-doctoral experience in Sydney, at the University of New South Wales.

Astrid Magenau received an MRes in Biology from University of Konstanz, Germany and a Ph.D. in Cell Biology from University of New South Wales Sydney, Australia concentrating on membrane organization during phagocytosis by macrophages. She now works at the Cellular Membrane Biology group, UNSW, Australia focusing on single molecule imaging (PAL-M) to study membrane organization during receptor activation.

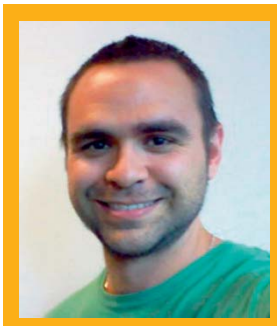

David Williamson received a BSc (Hons) in Pharmacology in 2002 from University of Western Australia. In 2003 he joined the Victor Chang Cardiac Research Institute in Sydney, Australia working in GPCR signaling. In 2006 he moved to the Centre for Vascular Research at the University of New South Wales, Sydney, Australia and since 2008 has been studying membrane biology and T-cell signaling for his Ph.D.

Macarena Rodriguez received a BSc Medical Science in 2001 at the University of Western Sydney and a BSc(Hons) in 2003 in the Developmental Neurobiology Unit at The Children's Medical Research Institute, Westmead Australia in association with UWS. She spent two years working as a research assistant in the Macrophage Biology Group at the University of New South Wales, Sydney before starting a Ph.D. in 2007 that aims to determine the role of membrane domains in sensing and regulating endothelial cell function when subjected to environmental conditions and changes to membrane lipid composition.

Associate Professor **Katharina Gaus** is a NHMRC Senior Research Fellow and leads the Membrane Biology Group at the Centre for Vascular Research, University of New South Wales. She received an MPhil in 1996 and a Ph.D. in 1999 both from the University of Cambridge, UK. The main objective of her research is to identify the principles that govern the organisation of the plasma membrane, and thus define the role of membrane domains in signal transduction processes.

References

[1] E. Betzig, G. H. Patterson, R. Sougrat, O. W. Lindwasser, S. Olenych, J. S. Bonifacino, M. W. Davidson, J. Lippincott-Schwartz, and H. F. Hess, Science **313**, 1642–1645 (2006).
[2] M. J. Rust, M. Bates, and X. Zhuang, Nat. Meth. **3**, 793–796 (2006).
[3] S. T. Hess, T. P. K. Girirajan, and M. D. Mason, Biophys. J. **91**, 4258–4272 (2006).
[4] N. C. Shaner, G. H. Patterson, and M. W. Davidson, J. Cell Sci. **120**, 4247–4260 (2007).
[5] G. U. Nienhaus, K. Nienhaus, A. Holzle, S. Ivanchenko, F. Renzi, F. Oswald, M. Wolff, F. Schmitt, C. Rocker, B. Vallone, W. Weidemann, R. Heilker, H. Nar, and J. Wiedenmann, Photochem. Photobiol. **82**, 351–358 (2006).
[6] D. Axelrod, J. Cell Biol. **89**, 141–145 (1981).
[7] M. Heilemann, S. van de Linde, M. Schüttpelz, R. Kasper, B. Seefeldt, A. Mukherjee, P. Tinnefeld, and M. Sauer, Angew. Chem. **47**, 6172–6176 (2008).
[8] M. Heilmann, S. van de Linde, A. Mukherjee, and M. Sauer, Angew. Chem. Int. Ed. **48**, 6903–6908 (2009).
[9] B. D. Ripley, J. R. Stat. Soc. Series B Stat. Methodol **39**, 172–192 (1977).
[10] M. A. Kiskowski, J. F. Hancock, and A. K. Kenworthy, Biophys. J. **97**, 1095–1103 (2009).
[11] I. A. Prior, C. Muncke, R. G. Parton, and J. F. Hancock, J. Cell Biol. **160**, 165–170 (2003).
[12] K. Gaus, E. Chklovskaia, B. Fazekas de St. Groth, W. Jessup, and T. Harder, J. Cell Biol. **171**, 121–131 (2005).
[13] S. Munro, Cell **115**, 377–388 (2003).
[14] C. R. F. Monks, B. A. Freiberg, H. Kupfer, N. Sciaky, and A. Kupfer, Nature **395**, 82–86 (1998).
[15] A. Grakoui, S. K. Bromley, C. Sumen, M. M. Davis, A. S. Shaw, P. M. Allen, and M. L. Dustin, Science **285**, 221–227 (1999).
[16] S. K. Bromley, W. R. Burack, K. G. Johnson, K. Somersalo, T. N. Sims, C. Sumen, M. M. Davis, A. S. Shaw, P. M. Allen, and M. L. Dustin, Annu. Rev. Immunol. **19**, 375–396 (2001).
[17] S. C. Bunnell, D. I. Hong, J. R. Kardon, T. Yamazaki, C. J. McGlade, V. A. Barr, and L. E. Samelson, J. Cell Biol. **158**, 1263–1275 (2002).
[18] R. Varma, G. Campi, T. Yokosuka, T. Saito, and M. L. Dustin, Immunity **25**, 117–127 (2006).
[19] G. Campi, R. Varma, and M. L. Dustin, J. Exp. Med. **202**, 1031–1036 (2005).
[20] M.-C. Seminario and S. C. Bunnell, Immunol. Rev. **221**, 90–106 (2008).
[21] T. Yokosuka, K. Sakata-Sogawa, W. Kobayashi, M. Hiroshima, A. Hashimoto-Tane, M. Tokunaga, M. L. Dustin, and T. Saito, Nat. Immunol. **6**, 1253–1262 (2005).
[22] G. L. W. Perry, Environ. Modell. Softw. **19**, 559–569 (2004)
[23] G. R. Chichili and W. Rodgers, J. Biol. Chem. **50**, 36682–36691 (2007).
[24] W. Rodgers, Biotechniques **32**, 1044–1051 (2002)
[25] R. E. Thompson, D. R. Larson, and W. W. Webb, Biophys. J. **82**, 2775–2783 (2002).

